How to cite: *Angew. Chem. Int. Ed.* **2021**, *60*, 1891 – 1896
International Edition: doi.org/10.1002/anie.202011494
German Edition: doi.org/10.1002/ange.202011494

**Metalloradicals**

# Ligand Protonation Triggers $H_2$ Release from a Dinickel Dihydride Complex to Give a Doubly "T"-Shaped Dinickel(I) Metallodiradical

*Peng-Cheng Duan[+], Roland Alexander Schulz[+], Anton Römer, Benjamin E. Van Kuiken, Sebastian Dechert, Serhiy Demeshko, George E. Cutsail III, Serena DeBeer, Ricardo A. Mata,* and Franc Meyer**

***Abstract:*** *The dinickel(II) dihydride complex (**1**$^{K}$) of a pyrazolate-based compartmental ligand with β-diketiminato (nacnac) chelate arms ($L^-$), providing two pincer-type {$N_3$} binding pockets, has been reported to readily eliminate $H_2$ and to serve as a masked dinickel(I) species. Discrete dinickel(I) complexes (**2**$^{Na}$, **2**$^{K}$) of $L^-$ are now synthesized via a direct reduction route. They feature two adjacent T-shaped metalloradicals that are antiferromagnetically coupled, giving an $S=0$ ground state. The two singly occupied local $d_{x^2-y^2}$ type magnetic orbitals are oriented into the bimetallic cleft, enabling metal–metal cooperative 2 $e^-$ substrate reductions as shown by the rapid reaction with $H_2$ or $O_2$. X-ray crystallography reveals distinctly different positions of the $K^+$ in **1**$^{K}$ and **2**$^{K}$, suggesting a stabilizing interaction of $K^+$ with the dihydride unit in **1**$^{K}$. $H_2$ release from **1**$^{K}$ is triggered by peripheral γ-C protonation at the nacnac subunits, which DFT calculations show lowers the barrier for reductive $H_2$ elimination from the bimetallic cleft.*

## Introduction

Nickel(I) complexes, while long considered rare and rather unstable,[1] are currently receiving much attention.[2] This is motivated not only by the mechanistic relevance of nickel(I) in some metalloprotein active sites (such as the cofactor F430 in methylcoenzyme M reductase or the Ni/Fe/S cofactor of acetyl coenzyme A synthase), but also by the increasing use of nickel(I) complexes in catalysis, most prominently in cross-coupling chemistry and in the reductive activation of small molecules.[3,4] For the latter, three-coordinate nickel(I) complexes with a "T"-shaped structure appear particularly promising, as they expose a reactive binding site with $d^9$ metalloradical character, with the unpaired electron residing in the accessible σ-antibonding $d_{x^2-y^2}$ orbital. This specific geometry can be enforced by pincer-type ligands, but structurally characterized systems are still rare; some prominent examples, **A**–**D**, are shown in Figure 1.[5–8] In contrast, β-diketiminato (nacnac) ligands with bulky N-substituents (**E**), which are most commonly employed in this field, usually give rise to the sterically more

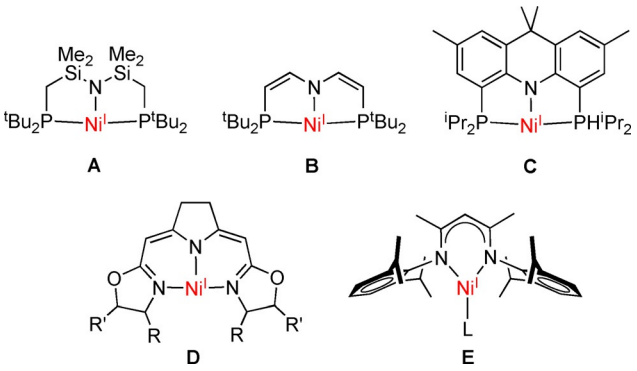


***Figure 1.*** Prominent examples of the few "T"-shaped $Ni^I$ complexes that have been structurally characterized by X-ray diffraction (see text for references).

[*] Dr. P.-C. Duan,[+] M. Sc. R. A. Schulz,[+] Dr. S. Dechert, Dr. S. Demeshko, Prof. Dr. F. Meyer
Universität Göttingen, Institut für Anorganische Chemie
Tammannstrasse 4, 37077 Göttingen (Germany)
E-mail: franc.meyer@chemie.uni-goettingen.de
Homepage: http://www.meyer.chemie.uni-goettingen.de

M. Sc. A. Römer, Prof. Dr. R. A. Mata
Universität Göttingen, Institut für Physikalische Chemie
Tammannstrasse 6, 37077 Göttingen (Germany)
E-mail: ricardo.mata@chemie.uni-goettingen.de

Dr. B. E. Van Kuiken, Dr. G. E. Cutsail III, Prof. Dr. S. DeBeer
Max Planck Institute for Chemical Energy Conversion (MPI-CEC)
Stiftstrasse 34–36, 45470 Mülheim an der Ruhr (Germany)

Prof. Dr. F. Meyer
Universität Göttingen, International Center for Advanced Studies of Energy Conversion (ICASEC)
Tammannstrasse 6, 37077 Göttingen (Germany)

Dr. P.-C. Duan[+]
New address: Center for Catalysis and Florida Center for Heterocyclic Compounds, Department of Chemistry, University of Florida
Gainesville, FL 32611-7200 (USA)

Dr. B. E. Van Kuiken
New address: European XFEL
Holzkoppel 4, 22869 Schenefeld (Germany)

[+] These authors contributed equally to this work.

Supporting information (general experimental details and characterization data for all of the reported compounds) and the ORCID identification number(s) for the author(s) of this article can be found under:
https://doi.org/10.1002/anie.202011494.

favored "Y"-shaped structures.[9–12] While all the above ligands generally form mononuclear nickel(I) complexes, Yoo and Lee recently pointed out that bimetallic versions of $(d_{x^2-y^2})^1$ based metalloradicals would be highly desirable for enabling two-electron transformations via metal-metal cooperativity (MMC).[7] This is well reflected in the various reactivities of complexes **A**–**E** that ultimately give dinickel(II) products composed of two {LNi} subunits;[3,4,7] however, binucleating scaffolds that preorganize two $d^9$ nickel(I) ions in a suitable arrangement for cooperative bimetallic chemistry are lacking.[13]

As most reductive transformations of small molecules (such as $CO_2$, $N_2$, etc.) involve the synchronized transfer of electron and protons, metal ligand cooperativity (MLC) exploiting proton transfer sites on the ligand has emerged a powerful concept[14] and has been well established for pincer scaffolds with N/NH groups in the backbone.[15] Non-innocence of β-diketiminato ligands at the γ-C atom has also been demonstrated, though it mostly involves oxygenative ligand modifications[16] or metal-ligand cross additions, while backbone protonation for enhancing the utility of nacnac complexes is relatively rare.[17]

We recently reported binucleating bis(tridentate) ligands that have two β-diketiminato compartments appended to a central pyrazolate bridge.[18] The dinickel(II) dihydride complexes $\mathbf{1^K}$ and **1′**, which are conveniently prepared from the dinickel(II) precursor $LNi^{II}_2Br$ and $KBEt_3H$ (Scheme 1),[18a] can be described as masked dinickel(I) synthons as they were shown to smoothly eliminate $H_2$ in the presence of substrates, enabling the two-electron reductive binding of various small molecules within the bimetallic cleft.[18,19] Intramolecular $H_2$ elimination is facile in case of **1′** at room temperature even in the absence of substrates, but has a much higher barrier in case of $K^+$-stabilized $\mathbf{1^K}$.[18a] The headspace GC/MS detection of $H_2$ released from solid samples of **1′** and in situ monitoring of the sample by SQUID magnetometry provided evidence for the formation of a highly reactive dinickel(I) intermediate **2′**.[18a]

Because of the topology of the two pincer-type $\{N_3\}$ binding compartments of $L^-$, complex **2′** was expected to feature two adjacent "T"-shaped nickel(I) subunits. The current work aimed at isolating and characterizing **2′** and at accessing such dinickel(I) complex of the binucleating β-diketiminato/pyrazolato hybrid ligand directly from $LNi_2Br$. During the course of these studies, it was found that $H_2$ release from $\mathbf{1^K}$ can be triggered by peripheral ligand protonation to give an unprecedented double "T"-shaped dinickel(I) complex that bears the potential of combining MMC and MLC reactivity in a bimetallic system.

## Results and Discussion

Attempts to crystallize the dinickel(I) complex **2′**, prepared by keeping samples of **1′** under vacuum for one day, yielded red crystals from THF/hexane. Unfortunately, despite many attempts the crystal quality of **2′** was only moderate, and insufficient for a neutron diffraction study. While X-ray diffraction (XRD) clearly confirmed the $\{LNi_2\}$ core structure, the absence or presence of hydride ligand within the bimetallic pocket could not be ascertained. A DFT optimized structure of the cation of **2′** (B3LYP-D3/def2-SVP; Figure 2a) indicated that all metric parameters are very similar in **1′** and **2′**. However, an NMR spectrum of the red product **2′** in $[D_8]$THF showed paramagnetism, and the Ni-H stretch at 1907 $cm^{-1}$ characteristic for **1′**[18a] is absent in the IR spectrum of solid **2′** (Figure S3). The nickel(I) character of **2′** was confirmed by X-ray absorption spectroscopy (XAS) (Fig-

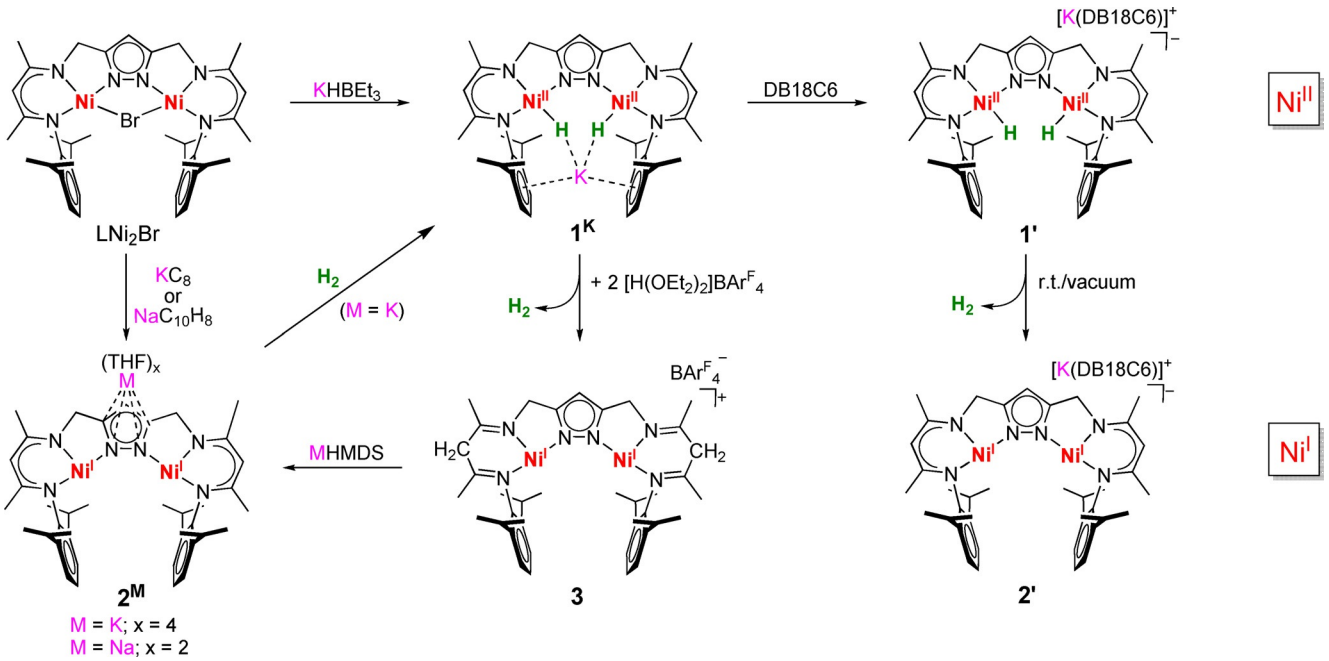


***Scheme 1.*** Overview of reactions towards dinickel(I) complexes studied in Ref. [18a] and in this work.

  

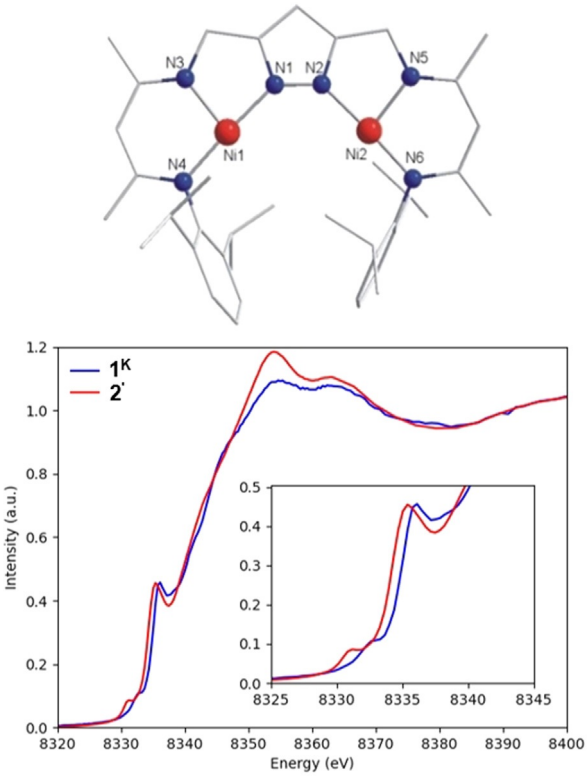


***Figure 2.*** Top: DFT-optimized structure of the anion of **2′** (B3LYP-D3/def2-SVP level). Hydrogen atoms are omitted for clarity. Bottom: Normalized Ni K-edge XAS spectra of complexes $\mathbf{1}^{K}$ and **2′**. The inset shows the low-energy features in the pre-edge and rising edge regions of the spectra.

ure 2b). Figure S40 shows the calculated Ni pre-edge spectra of complexes $\mathbf{1}^{K}$ and **2′** compared with the experimental data. Difference densities provide a depiction of the spatial distribution of the core excited electrons, and for complexes $\mathbf{1}^{K}$ and **2′** they are distributed in the equatorial plane of the complex and reveal that the pre-edge features are due to the $1s \rightarrow d_{x^2-y^2}$ transition. The calculated spectra show a $\approx 1.3$ eV decrease in pre-edge energy on going from complex $\mathbf{1}^{K}$ to **2′**, which is in good agreement with the observed shift in the experimental pre-edge energies, corroborating that **2′** is a nickel(I) species.

An alternative synthetic route to obtain a $\{LNi^{I}_{2}\}$ species directly, circumventing the dihydride intermediate, could now be established by treating the precursor complex $LNi_2Br$ with strong reducing agents such as $KC_8$ or sodium naphthalenide in THF. Single crystals of highly air and moisture sensitive $\mathbf{2}^{M}$ (M = Na or K) suitable for X-ray diffraction were obtained by layering THF solutions of the products with hexane/$Et_2O$ at −30 °C and after several recrystallizations; the molecular structure of $\mathbf{2}^{K}$ is shown in Figure 3(see SI for the structure of $\mathbf{2}^{Na}$ and for crystallographic details as well as a complete list of bond lengths and angles). It confirms the presence of two NNN-based "T"-shaped nickel(I) subunits that are spanned by the pyrazolate with $d(Ni\cdots Ni) = 4.1243(7)$ Å and with angles N1-Ni1-N4 and N2-Ni2-N6 very close to 180° (viz. 176.8(1) and 176.2(1)°). Comparison of the molecular structures of $K[LNi^{I}_{2}]$ ($\mathbf{2}^{K}$) and $K[L(Ni^{II}\text{-}H)_2]$ ($\mathbf{1}^{K}$) shows that the

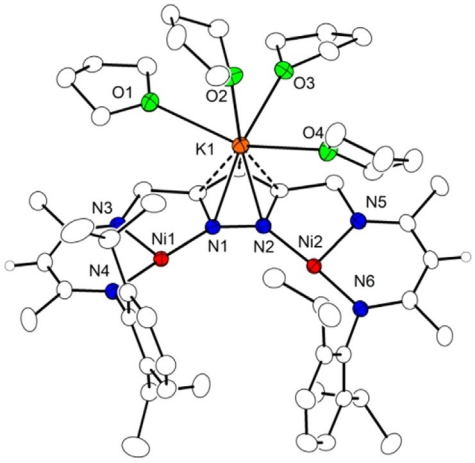


***Figure 3.*** Molecular structure of $\mathbf{2}^{K}$ (30% probability thermal ellipsoids). $K^{+}\cdots C^{pz}$ contacts < 3.5 Å are shown as dashed lines.[24]

most conspicuous difference is the position of the $K^+$ cation: In $\mathbf{1}^{K}$ the $K^+$ is located within the plane defined by the pyrazolate-bridged dinickel dihydride core and in between the two flanking aryl rings of the 2,6-disopropylphenyl (dipp) substituents at distances indicative of cation-π interactions.[18a] In contrast, in $\mathbf{2}^{K}$ the $K^+$ is located above the pyrazolate[20] and is additionally ligated by four THF molecules (the structure of $\mathbf{2}^{Na}$ is very similar, but the $Na^+$ has only two THF ligands; Figure S9). This striking difference may reflect attractive $K^+\cdots$hydride interactions in $\mathbf{1}^{K}$ that are now absent in the double "T"-shaped dinickel(I) complex $\mathbf{2}^{K}$, in line with the stabilizing role of $K^+$ with respect to $H_2$ elimination from $\mathbf{1}^{K}$ which has a much higher activation barrier than $H_2$ elimination from **1′**.

The dinickel(I) character of $\mathbf{2}^{K}$ (and $\mathbf{2}^{Na}$) was confirmed by magnetic susceptibility measurements (Figure 4; see SI for details). SQUID data for a sample of crystalline material of $\mathbf{2}^{K}$ show a $\chi_M T$ value of 0.66 $cm^3 mol^{-1} K$ at 270 K and a decrease of $\chi_M T$ upon lowering the temperature, approaching zero below 30 K. This reflects significant antiferromagnetic coupling and an $S_T = 0$ ground state. Analysis of the magnetic data using a dimer model with two coupled $S = {}^1/_2$ spin centers ($\hat{H} = -2J\hat{S}_1\hat{S}_2$ Hamiltonian; see SI for details) gave $J = -71\ cm^{-1}$ ($g = 2.14$), in excellent agreement with $J = -69.5\ cm^{-1}$ derived from the magnetic data of **2′** that was prepared by keeping crystals of **1′** under vacuum for 15 h.[18a] Antiferromagnetic coupling is slightly stronger in $\mathbf{2}^{Na}$ ($J = -83\ cm^{-1}$; see Figure S8), which may be related to the more planar pyrazolato-based dinickel(I) core: the torsion angle Ni(1)-N(1)-N(2)-Ni(2) is 4.9° in $\mathbf{2}^{Na}$ versus 18.2° in $\mathbf{2}^{K}$. Note that the $M\text{-}N^{pz}\text{-}N^{pz}\text{-}M$ torsion has previously been shown to have a strong effect on the magnetic coupling in pyrazolato-bridged complexes of two $S = {}^1/_2$ metal ions M,[21] and the coupling may even become ferromagnetic in orthogonal situations when the torsion approaches 90°.[22]

Distances and angles of the DFT optimized structures of $[LNi_2]^-$ (viz. the anion of $\mathbf{2}^{M}$ and **2′**) are in good agreement with metric parameters observed experimentally (Table S3). Energies of the $S = 1$ and the antiferromagnetically coupled broken symmetry state differ by less than 0.2 kcal $mol^{-1}$

  

(Table S5) and optimized structures are almost identical. A single point calculation based on the atomic coordinates taken from the X-ray crystallographic analysis of $\mathbf{2^K}$ confirms an antiferromagnetically coupled ground state ($J \approx -100\ cm^{-1}$; Table S5). According to a Löwdin spin population analysis 87% of the spin density is located on the nickel ions (a spin density plot is shown in Figure S19). The magnetic orbitals (from unrestricted corresponding orbitals; see inset in Figure 4) have mainly nickel d character, viz. ≈70% according to Löwdin reduced orbital populations per MO, with only minor contributions from nickel s- and p-orbitals (<10%). The small calculated overlap (0.05) of the corresponding orbitals is in agreement with weak antiferromagnetic coupling.[23]

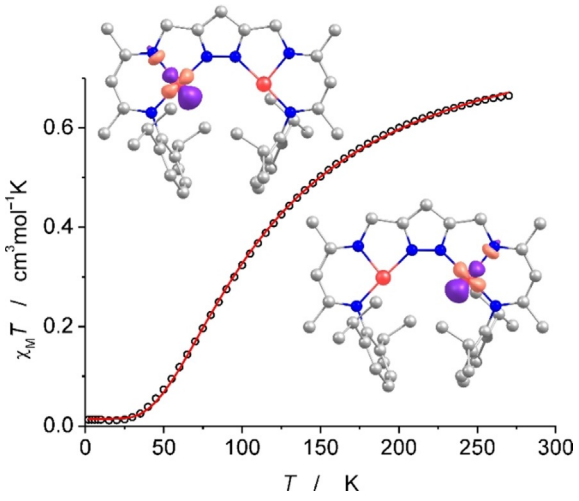


***Figure 4.*** $\chi_M T$ versus $T$ plot for $\mathbf{2^K}$; the solid red line is the calculated curve fit ($\hat{H} = -2J\hat{S}_1\hat{S}_2$ with $J = -71\ cm^{-1}$ and $g = 2.14$). The insets show the magnetic orbitals according to DFT calculations (see text and Supporting Information for details).

The magnetic orbitals of $[LNi_2]^-$ are best described as the local σ-antibonding $d_{x^2-y^2}$ orbitals of the metalloradical subunits, similar to the SOMO in mononuclear T-shaped nickel(I) complexes.[7] In $[LNi_2]^-$ these half-filled orbitals are oriented into the bimetallic cleft, suggesting that metal-metal cooperative $2e^-$ substrate transformations within the cleft should be facile. Indeed, $\mathbf{2^K}$ smoothly reacts with $H_2$ to give $\mathbf{1^K}$ via homolytic σ-bond cleavage (see Scheme 1), and it rapidly reacts with $O_2$ to give the $\mu_{1,2}$-peroxo complex $[KLNi_2(O_2)]$.[19a]

To probe whether $H_2$ release from the $K^+$-stabilized dihydride complex $\mathbf{1^K}$ can be induced by protonation, a THF solution of $\mathbf{1^K}$ was treated with $[H(OEt_2)_2]BAr^F{}_4$. This causes an immediate color change of the solution from orange to brown-red, accompanied by gas evolution. Single crystals of the highly air and moisture sensitive product **3** were obtained by layering the THF solution with hexane/$Et_2O$ at −30 °C. The molecular structure of the cation of **3** determined by X-ray diffraction is shown in Figure 5 (see SI for further details). In **3**, the two nickel ions are again found tricoordinate in nearly perfect "T"-shaped geometry (N-Ni-N angles of 84.6°, 97.0° and 177.9° at Ni1 and 84.6°, 96.5° and 178.0° at Ni2) at

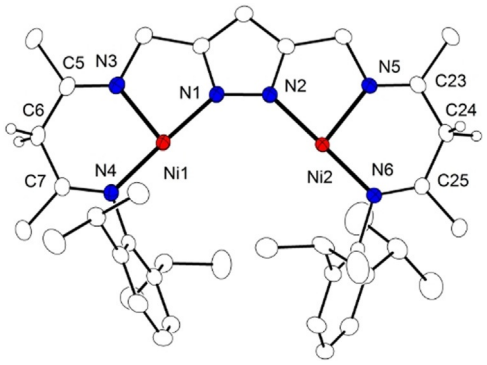


***Figure 5.*** Molecular structure of $[L^{H2}Ni^I_2]^+$ (cation of **3**; thermal ellipsoids set at 30% probability). The $BAr^F{}_4$ counteranion and most hydrogen atoms (except for those at the γ-C of the β-diimine subunits) are omitted for clarity.[24]

a distance of $d(Ni\cdots Ni) = 4.1032(5)$ Å. Both nacnac parts are protonated at the γ-C atoms, and the presence of two β-diimine subunits in $[L^{H2}Ni^I_2]^+$ (cation of 3) is evidenced by short C=N bonds (average 1.285(3) Å in 3 vs. 1.330(3) Å in $\mathbf{1^K}$ or 1.332(5) Å in $\mathbf{2^K}$) and by a characteristic C=N stretch at 1670 $cm^{-1}$ in the IR spectrum.

A DFT optimized structure of $[L^{H2}Ni^I_2]^+$ reproduces well the experimentally determined metric parameters of the cation of **3** (Table S4), and the computational results indicate an $S = 0$ ground state with antiferromagnetic coupling of the same magnitude as in $[LNi_2]^-$ (Table S5). UV-vis spectra of $\mathbf{2^K}$, $\mathbf{2^{Na}}$ and **3** in THF show quite intense bands in the range 350–400 nm typical for all dinickel complexes of the binucleating ligand $L^-$. The present dinickel(I) complexes show broad low-energy shoulders around 450 nm, and $\mathbf{2^K}$ features an additional weak absorption around 520 nm (Figure 6). According to TD-DFT computations these absorptions at lower energy beyond 420 nm are mostly assigned to metal to ligand charge transfer (MLCT) transitions involving the nacnac or β-diimine parts of the ligand, respectively.

When the dideuteride analogue of $\mathbf{2^K}$, $[KL(Ni^{II}\text{-}D)_2]$ ($\mathbf{1^K\text{-}D}$), was protonated with 2 equivalents of $[H(Et_2O)_2]BAr^F{}_4$ in THF and the reaction monitored by $^2H$ NMR spectroscopy, clean formation of $D_2$ was detected, without any signs of HD

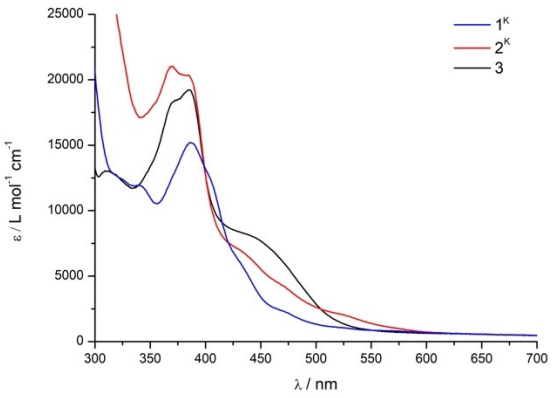


***Figure 6.*** UV/Vis spectra of dinickel(II) complex $\mathbf{1^K}$ and dinickel(I) complexes $\mathbf{2^K}$ and **3** in THF at room temperature.

  

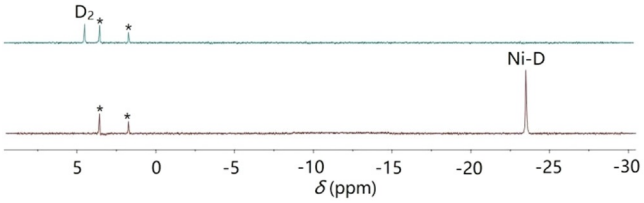


***Figure 7.*** $^2$H NMR spectrum (77 MHz) of a solution of $\mathbf{1^K}$**-D** in THF (bottom) and after addition of 2 equivalents of [H-($Et_2O$)$_2$]$BAr^F{}_4$ (top); solvent signals are marked with an asterisk.

(Figure 7). This shows that only the Ni-bound hydride (deuteride) ligands are released, and it suggests that protonation at the peripheral γ-C atoms triggers intramolecular reductive elimination of $H_2$ ($D_2$) from the bimetallic cleft.

The paths to reductive $H_2$ release were then computed with and without protonation of the peripheral ligand, starting from the structures of the anion $\mathbf{1'}$ and the hypothetical dihydride of **3**, $[L^{H2}(Ni\text{-}H)_2]^+$ ($\mathbf{3'}$); the results are depicted in Figure 8a. By bringing the two hydrogen atoms closer together in a constrained optimization path, one crosses from the dihydride (MIN1) to a pre-dissociated state (MIN2), separated by a small barrier (TS1). As in the previous report on $\mathbf{1^K}$ and $\mathbf{1'}$,[18a] we estimate the last barrier to $H_2$ release from the bimetallic cleft with the equilibrium dihydrogen H-H distance at the same level of theory (TS2*). An energy plateau MIN2 is observed (viz., formation of the dihydrogen bond). One notable difference between $\mathbf{1'}$ and $\mathbf{3'}$ is the depth of MIN2, which is significantly stabilized upon protonation of the nacnac-type ligand subunits. At the level of theory used, this minimum is as stable as the starting dihydride complex (MIN1). The TS2 barrier towards final $H_2$ release is also significantly reduced upon peripheral ligand protonation (from about 55 to 37 kJ mol$^{-1}$). When considering the same pathways with a $K^+$ cation in the pocket, $H_2$ release is again favored in the case of $\mathbf{3^{K\prime}}$ compared to $\mathbf{1^K}$. In this case a new factor comes into play: the added flexibility of the protonated ligand $[L^{H2}]^-$ upon loss of the conjugation in the β-diimine subunits. The tridentate pincers can now move above the plane with the cation, opening a path for $H_2$ to leave the complex. We show a comparison of the two computed minima structures of $\mathbf{1^K}$ and $\mathbf{3^{K\prime}}$ in Figures 8b and c, respectively, where the effect is clearly visible.

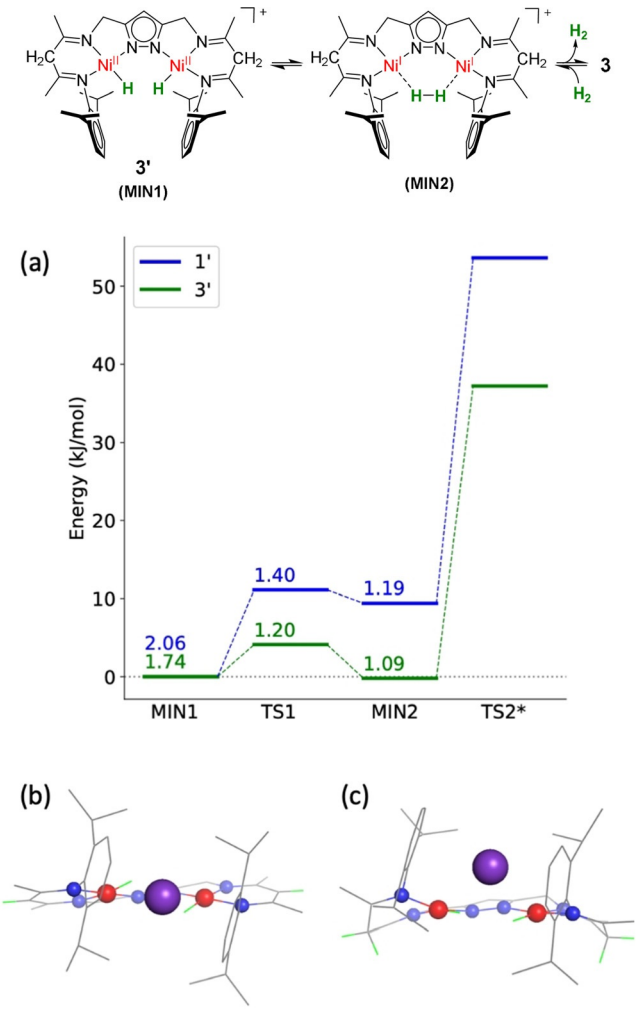


***Figure 8.*** a) Computed reaction paths (electronic energies) for $H_2$ release. The numbers above the bars indicate the H–H distance at each stationary point. TS2* is an approximation to the barrier for hydrogen release, obtained by performing a constrained optimization at the equilibrium dihydrogen distance (see Supporting Information). The optimized structures of b) $\mathbf{1^K}$ and c) $[L^{H2}(Ni\text{-}H)_2K]^{2+}$ (cation of $\mathbf{3^{K\prime}}$). Both the leaving hydrogen atoms and the ones at the γ-C of the β-diimine subunits are shown as bright green sticks.

## *Conclusion*

In conclusion, using a pyrazolate-based ligand scaffold that provides two pincer-type {$N_3$} binding compartments a relatively stable dinickel(I) complex featuring two adjacent T-shaped metalloradicals has been isolated and comprehensively characterized, including magnetic measurements that reveal moderate antiferromagnetic coupling and an $S=0$ ground state. The two singly occupied $d_{x^2-y^2}$ type magnetic orbitals of the $d^9$ nickel(I) subunits are quite exposed and both oriented into the bimetallic cleft, which promises rich metal-metal cooperative 2e$^-$ chemistry as evidenced by the rapid reaction of $\mathbf{2^K}$ with $H_2$ or $O_2$ to give the dinickel(II) dihydride or dinickel(II) peroxide species $[KL(Ni\text{-}H)_2]$ ($\mathbf{1^K}$) and $[KLNi_2(O_2)]$, respectively. Pincer-based T-shaped nickel(I) metalloradicals have recently been shown to serve as powerful reductants for challenging substrate activations,[3,4,6,7] and the present system now provides a highly preorganized dinuclear variant that can capture 2e$^-$-reduced substrates within its bimetallic pocket. Interestingly, the molecular structures of $[KL(Ni^{II}\text{-}H)_2]$ ($\mathbf{1^K}$) and $[KL(Ni^{I})_2]$ ($\mathbf{2^K}$) differ by the position of the $K^+$ cation, supporting a stabilizing effect of the $K^+$ on the dihydride unit. We have previously reported that dinickel(II) dihydride complexes $\mathbf{1^K}$ and $\mathbf{1'}$ serve as masked synthons for a highly reactive dinickel(I) species,[18] and it is now demonstrated that dehydrogenation can be triggered by peripheral ligand protonation, which drastically lowers the barrier for reductive $H_2$ elimination from the bimetallic cleft. This finding also emphasizes the non-innocence of nacnac ligands in terms of

  

metal-ligand cooperativity. It is an exciting perspective that $[L^{H2}Ni^{I}_{2}]^{+}$ (**3**) offers not only two $e^{-}$ (as a highly reactive dimetallodiradical), but also two $H^{+}$ (stored at the ligand periphery) to potentially mediate coupled $2e^{-}/2H^{+}$ substrate transformations. Work in this direction is in progress in our laboratory.

## Acknowledgements

Support from the China Scholarship Council (Ph.D. fellowship for P.-C.D.) and the University of Göttingen (F.M.) is gratefully acknowledged. S.DeBeer acknowledges the Max Planck Society for financial support. This project has been partly funded by the Deutsche Forschungsgemeinschaft (DFG, German Research Foundation)—project number 405832858 (computing cluster) and 423268549 (X-ray diffractometer). Use of the Stanford Synchrotron Radiation Lightsource, SLAC National Accelerator Laboratory, is supported by the U.S. Department of Energy, Office of Science, Office of Basic Energy Sciences under Contract No. DE-AC02-76SF00515. The SSRL Structural Molecular Biology Program is supported by the DOE Office of Biological and Environmental Research, and by the National Institutes of Health, National Institute of General Medical Sciences (P41GM103393). Open access funding enabled and organized by Projekt DEAL.

## Conflict of interest

The authors declare no conflict of interest.

**Keywords:** dinuclear complexes · ligand protonation · magnetic properties · metalloradicals · nickel(I)

[1] F. Meyer, H. Kozlowski in *Comprehensive Coordination Chemistry II*, *Vol. 6* (Eds.: J. A. McCleverty, T. J. Meyer), Elsevier, Oxford, **2004**, pp. 247 – 554.
[2] C.-Y. Lin, P. P. Power, *Chem. Soc. Rev.* **2017**, *46*, 5347 – 5399.
[3] S. Yao, M. Driess, *Acc. Chem. Res.* **2012**, *45*, 276 – 287.
[4] P. Zimmermann, C. Limberg, *J. Am. Chem. Soc.* **2017**, *139*, 4233 – 4242.
[5] M. J. Ingleson, B. C. Fullmer, D. T. Buschhorn, H. Fan, M. Pink, J. C. Huffman, K. G. Caulton, *Inorg. Chem.* **2008**, *47*, 407 – 409.
[6] F. Schneck, J. Ahrends, M. Finger, A. C. Stückl, C. Würtele, D. Schwarzer, S. Schneider, *Nat. Commun.* **2018**, *9*, 1161.
[7] C. Yoo, Y. Lee, *Angew. Chem. Int. Ed.* **2017**, *56*, 9502 – 9506; *Angew. Chem.* **2017**, *129*, 9630 – 9634.
[8] a) C. A. Rettenmeier, H. Wadepohl, L. H. Gade, *Chem. Eur. J.* **2014**, *20*, 9657 – 9665; b) C. A. Rettenmeier, H. Wadepohl, L. H. Gade, *Chem. Sci.* **2016**, *7*, 3533 – 3542.
[9] a) P. L. Holland, T. R. Cundari, L. L. Perez, N. A. Eckert, R. J. Lachicotte, *J. Am. Chem. Soc.* **2002**, *124*, 14416 – 14424; b) N. A. Eckert, A. Dinescu, T. R. Cundari, P. L. Holland, *Inorg. Chem.* **2005**, *44*, 7702 – 7704.
[10] E. Kogut, H. L. Wiencko, L. Zhang, D. E. Cordeau, T. H. Warren, *J. Am. Chem. Soc.* **2005**, *127*, 11248 – 11249.
[11] G. Bai, P. Wei, D. W. Stephan, *Organometallics* **2005**, *24*, 5901 – 5908.
[12] a) S. Pfirrmann, S. Yao, B. Ziemer, R. Stößer, M. Driess, C. Limberg, *Organometallics* **2009**, *28*, 6855 – 6860; b) S. Pfirrmann, C. Limberg, B. Ziemer, *Dalton Trans.* **2008**, 6689 – 6691; c) S. Pfirrmann, C. Limberg, C. Herwig, C. Knispel, B. Braun, E. Bill, R. Stösser, *J. Am. Chem. Soc.* **2010**, *132*, 13684 – 13691; d) P. Holze, B. Braun-Cula, S. Mebs, C. Limberg, *Z. Anorg. Allg. Chem.* **2018**, *644*, 973 – 981.
[13] T. Inatomi, Y. Koga, K. Matsubara, *Molecules* **2018**, *23*, 140.
[14] a) J. R. Khusnutdinova, D. Milstein, *Angew. Chem. Int. Ed.* **2015**, *54*, 12236 – 12273; *Angew. Chem.* **2015**, *127*, 12406 – 12445; b) D. G. A. Verhoeven, M.-E. Moret, *Dalton Trans.* **2016**, *45*, 15762 – 15778.
[15] a) P. A. Dub, J. C. Gordon, *ACS Catal.* **2017**, *7*, 6635 – 6655; b) L. Alig, M. Fritz, S. Schneider, *Chem. Rev.* **2019**, *119*, 2681 – 2751.
[16] P. Holze, T. Corona, N. Frank, B. Braun-Cula, C. Herwig, A. Company, C. Limberg, *Angew. Chem. Int. Ed.* **2017**, *56*, 2307 – 2311; *Angew. Chem.* **2017**, *129*, 2347 – 2351.
[17] C. Camp, J. Arnold, *Dalton Trans.* **2016**, *45*, 14462 – 14498.
[18] a) D.-H. Manz, P.-C. Duan, S. Dechert, S. Demeshko, R. Oswald, M. John, R. A. Mata, F. Meyer, *J. Am. Chem. Soc.* **2017**, *139*, 16720 – 16731; b) H. Stevens, P.-C. Duan, S. Dechert, F. Meyer, *J. Am. Chem. Soc.* **2020**, *142*, 6717 – 6728.
[19] a) P.-C. Duan, D.-H. Manz, S. Dechert, S. Demeshko, F. Meyer, *J. Am. Chem. Soc.* **2018**, *140*, 4929 – 4939; b) E. Ferretti, S. Dechert, S. Demeshko, M. C. Holthausen, F. Meyer, *Angew. Chem. Int. Ed.* **2019**, *58*, 1705 – 1709; *Angew. Chem.* **2019**, *131*, 1719 – 1723; c) E. Ferretti, S. Dechert, F. Meyer, *Inorg. Chem.* **2019**, *58*, 5154 – 5162; d) T. Kothe, U.-H. Kim, S. Dechert, F. Meyer, *Inorg. Chem.* **2020**, *59*, 14207 – 14217.
[20] A similar bonding situation for $K^{+}$ countercations has been found previously in anionic pyrazolato-bridged bimetallic complexes; see, e.g.: C. J. Röder, F. Meyer, E. Kaifer, *Angew. Chem. Int. Ed.* **2002**, *41*, 2304 – 2306; *Angew. Chem.* **2002**, *114*, 2414 – 2417.
[21] D. Ajò, A. Bencini, F. Mani, *Inorg. Chem.* **1988**, *27*, 2437 – 2444.
[22] a) L. K. Frensch, K. Pröpper, M. John, S. Demeshko, C. Brüchner, F. Meyer, *Angew. Chem. Int. Ed.* **2011**, *50*, 1420 – 1424; *Angew. Chem.* **2011**, *123*, 1456 – 1460; b) N. Kindermann, E. Bill, S. Dechert, S. Demeshko, E. J. Reijerse, F. Meyer, *Angew. Chem. Int. Ed.* **2015**, *54*, 1738 – 1743; *Angew. Chem.* **2015**, *127*, 1758 – 1763.
[23] F. Neese, *J. Phys. Chem. Solids* **2004**, *65*, 781 – 785.
[24] Deposition Number(s) 2016725, 2016726, and 2016727 contain the supplementary crystallographic data for this paper. These data are provided free of charge by the joint Cambridge Crystallographic Data Centre and Fachinformationszentrum Karlsruhe Access Structures service www.ccdc.cam.ac.uk/structures.

Manuscript received: August 21, 2020
Accepted manuscript online: October 7, 2020
Version of record online: November 24, 2020

  